

# Large-Amplitude Rotary Induced-Strain (LARIS) Actuator

VICTOR GIURGIUTIU\* AND CRAIG A. ROGERS

*College of Engineering, University of South Carolina, Columbia, SC 29208*

**ABSTRACT:** Induced-strain materials can produce very large forces and, hence, large energy density, but small actual displacements. A new concept for obtaining large-amplitude rotary displacements from small linear displacements generated by induced-strain material stacks is proposed. The concept utilizes the theory of twist-warping coupling in thin-wall open tubes. The theory of the proposed solid-state axial-to-rotary converter-amplifier, together with the appropriate bibliographical references, is given. A simple formula is generated for estimating the axial-to-rotary conversion-amplification coefficient from the geometrical length,  $L$ , and enclosed area,  $A$ , of the open tube. A large-displacement induced-strain rotary (LARIS) actuator proof-of-concept demonstrator was built and tested to verify and validate the theoretical developments. The LARIS actuator consisted of a 28 mm diameter, 1.2 m length open tube and a  $120\ \mu\text{m}$ ,  $-1000\ \text{V}$  PZT translator. The experimental set-up and the excitation and measuring equipment are fully described in the paper. A maximum rotary displacement of  $8^\circ$  was measured, and the linear relationship between the rotation coefficient, the tube length,  $L$ , and the inverse of the enclosed area,  $A$ , was verified. An improved theoretical model, that accounts for the experimentally observed zero off-set, is also given.

The theoretical developments and experimental tests presented in this paper show that the proposed LARIS actuator, based on a novel solid-state axial-to-rotary converter-amplifier utilizing the warping-torsion coupling of an open tube, is a viable design option, of great constructive simplicity and very low parts count. This concept can be successfully used in a series of aerospace and mechanical engineering applications, as for example in the actuation of adaptive control surfaces for aircraft wings and helicopter blades. The  $8^\circ$  rotary displacement capabilities measured on the proof-of-concept demonstrator can be easily scaled to other values to meet the operation requirements of specific applications. For very large angles ( $40\text{--}50^\circ$ ), conventional electro-mechanical actuators (e.g., stepper-motors and ball-screws assemblies) can be used.

## INTRODUCTION

**S**SOLID-STATE induced-strain actuators present outstanding advantages over conventional electro-mechanical and hydraulic actuation options due to their compact construction, very low parts count and potentially high reliability. The development of solid-state induced-strain actuators (ISA) has entered the production stage, and actuation devices based on these concepts are likely to reach the applications market in the next few years. An increasing number of vendors are producing and marketing solid-state actuation devices based on induced-strain principles (Giurgiutiu, Chaudhry, and Rogers, 1996). Induced-strain materials can produce very large forces and, hence, large energy density, but small actual displacements. For most practical applications, amplification of the induced-strain displacement must be performed in an effective way which preserves as much as possible the induced-strain energy. For rotary actuation, an additional mechanism must be provided to convert the linear induced-strain displacement into angular stroke output. As shown by Giurgiutiu et al. (1994), conventional approaches to displacement amplification and the linear-to-rotary conversion consume large proportions of the induced-strain effect and thus

greatly reduce the overall effectiveness of the actuator. For example, the bimorph piezoelectric actuators obtain appreciable bending displacements, but have a very restricted force capability and an inefficient strain distribution across the thickness. Spangler and Hall (1990) and Samak and Chopra (1993) used bimorph PZT actuators, rotor arms, and linkages to produce the rotation of a trailing edge flap, but did not obtain satisfactory experimental results. Barrett, Gross, and Brozoski (1995) developed an active bending device (flexspar) coupled to an internally-built rotor arm to achieve large rotations of all-moving missile fins. Ingenious aerodynamic and aeroelastic control had to be used in order to use the airstream forces for augmenting the angular displacement of the fins.

Giurgiutiu et al. (1994) demonstrated that the use of stack actuators is much more efficient than other proposed induced-strain options since the induced-strain effect is utilized uniformly across the layer thickness. Spencer and Chopra (1996) used piezoelectric stacks to drive a trailing edge flap, through a lever amplification and rotor arm axial-to-rotational converter. Delicate miniaturization and large lever ratios were used to achieve satisfactory amplification ratios and relatively large angular displacements ( $3.5^\circ$ ) under no-load conditions. However, when aerodynamic loads were applied, the deflection decreased gradually to  $1.5^\circ$ . This decrease could be

\*Author to whom correspondence should be addressed.

attributed to the deflection loss due to lever arm and support flexibility, and to kinematic play in the linkage joints. Fenn et al. (1993) proposed a flap actuation system using magneto-active TERFENOL rods, a deformable-triangle displacement amplifier, and a rotor arm. Straub and King (1996) are constructing a full-scale flap actuation system utilizing piezoelectric stacks, levers (bell cranks) and linkages for the MD900 helicopter.

Solid-state devices have the advantages that no displacement loss takes place in the linkage joints. Solid-state devices for axial-to-rotary conversion have been proposed by several authors. Chen and Chopra (1993) used PZT crystals applied at  $\pm 45^\circ$  to induced twist in an airfoil section, but the measure rotation did not exceed  $0.5^\circ$ . Bothwell, Chandra, and Chopra (1994) tested extension-torsion coupled composite tubes driven by magneto-active TERFENOL rods, and reported angular displacements around  $0.2^\circ$ . Bernhard and Chopra (1996) experimented with bending-torsion coupled composite beams incorporating PZT elements, and measured maximum rotations around  $0.5^\circ$ . These values are about an order of magnitude less than the values required to achieve meaningful practical results. The inability of these solid-state devices to achieve large angular displacement can be traced to a common cause: they all utilize closed-tube constructions that have inherently high torsional stiffness, and hence are difficult to deform.

A completely different approach is taken in the design outlined in the present paper: instead of using inherently-stiff closed tubes, the use of inherently-flexible open tubes is proposed. We also propose to combine the axial-to-rotary converter and displacement amplifier into one solid-state device. To achieve this, the large-displacement induced-strain rotary (LARIS) actuator presented in this paper utilizes an unexplored application of basic solid-mechanics principles. Thus, a unified solution to the induced-strain rotary actuation problem is achieved. The displacement amplification and the linear-to-rotary transformation are combined into one solid-state construction that can be manufactured from conventional or composite materials, as the need arises. An explicit design procedure allows the designer to adjust the shape and geometry of the device to meet the requirements of specific applications. For other applications, the device operation can be further enhanced by using composite materials with tailored properties. Experimental trials of the proposed concept, performed in the laboratory of the Center for Intelligent Material Systems and Structures (CIMSS) at Virginia Polytechnic Institute and State University (Virginia Tech) with an inexpensive proof-of-concept demonstrator and commercially-available equipment, have demonstrated large displacement capabilities ( $\delta = 8^\circ$ ) with stable and predictable behavior.

It should be also pointed out that the open-tube actuation solution proposed in this paper is not a good-for-all *panacea*. For the same geometry and wall thickness, open tubes are more flexible in torsion than closed tubes, and they can bear less torsional loads. These effects, though drawbacks, can be

compensated through the use of different wall thickness and/or high-performance composite materials with orthotropic properties. Tailoring of composite material properties coupled with design optimization would present a worthwhile extension of the present analysis.

## THEORETICAL BACKGROUND

### Basic Equations of Linear Electro-Active Material Behavior

The general constitutive equations of linear electro-active material behavior, given by ANSI/IEEE Standard 176-1987, describe a tensorial relation between mechanical and electrical variables (mechanical strain  $S_{ij}$ , mechanical stress  $T_{ij}$ , electrical field  $E_i$ , and electrical displacement  $D_i$ ) in the form:

$$S_{ij} = s_{ijkl}^E T_{kl} + d_{kij} E_k \quad (1)$$

$$D_j = d_{jkl} T_{kl} + \epsilon_{jk}^T E_k$$

where  $s_{ijkl}^E$  is the mechanical compliance of the material measured at zero electric field ( $E = 0$ ),  $\epsilon_{jk}^T$  is the dielectric permittivity measured at zero mechanical stress ( $T = 0$ ), and  $d_{kij}$  is the piezo-electric coupling between the electrical and mechanical variables. The second equation reflects the *direct piezo-electric effect*, while the first equation refers to the *converse piezo-electric effect*.

Typical electro-active induced-strain actuators are stacks of thin active-material layers, alternatingly charged (Figure 1). In such an electro-active material stack, mechanical stress and electric field act only in the 3-direction (the stack axis), and the transverse effects can be neglected in a first-order analysis. The one-dimensional equivalent of Equations (1) is, simply,

$$S = s \cdot T + d \cdot E \quad (1a)$$

$$D = d \cdot T + \epsilon \cdot E$$

where the subscripts "3," "33," "333," and "3333" are implied, as appropriate. The compliance,  $s$ , is assumed to be measured at zero electric field, while the permittivity,  $\epsilon$ , is measured at zero stress.

### Basic Equations of Twist-Warping Coupling in Thin Open Tubes

#### STRAIN-DISPLACEMENT ANALYSIS

Consider a thin-wall cylinder of non-circular, open cross-section (open tube) as shown in Figure 2. Choose an orthogonal system of axes  $Oxyz$ , with the  $z$  axis along the cylinder axis. Along the  $x$ ,  $y$ ,  $z$  axes, define the deformation displacements,  $u$ ,  $v$ ,  $w$ , respectively. Assume that the tube is loaded and/or constrained only at its ends, and hence its strain field is uniform along the  $z$  axis. Hence, its state of deformation is

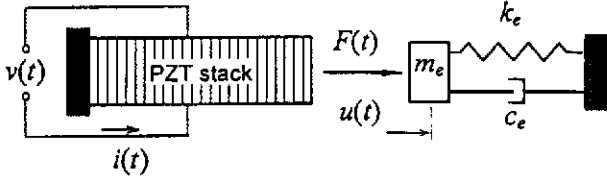


Figure 1. Schematic representation of a solid-state induced-strain actuator (PZT stack) operating against a mechanical load.

self-similar along the  $z$  axis. Under torsional deformation, initially plane sections in the tube undergo rotation,  $\beta(z)$ , and warping,  $w(x,y,z)$ . Denoting by  $\vec{u} = u\vec{i} + v\vec{j} + w\vec{k}$  the displacement vector of a generic point P of position vector  $\vec{r} = x\vec{i} + y\vec{j} + z\vec{k}$ , we write:

$$\vec{u} = [\beta(z)\vec{k}] \times \vec{r} + w(x,y,z)\vec{k} \quad (2)$$

Since the deformation is self-similar along the  $z$  axis, the rate of twist,  $\theta = d\beta/dz$ , is constant and proportional to the external loading. Thus,  $\beta(z) = \theta z$ . The warping is assumed to be the product of a self-similar function,  $\psi(x,y)$ , that depends only on the cross-sectional geometry, and the rate of twist,  $\theta$ . Hence, Equation (2) becomes:

$$\begin{aligned} u(x,y,z) &= -\theta \cdot zy \\ v(x,y,z) &= \theta \cdot zx \\ w(x,y,z) &= \theta \cdot \psi(x,y) \end{aligned} \quad (3)$$

Using the fundamental definition of strain [ $\epsilon_{xx} = \partial u/\partial x$ ,  $\epsilon_{yy} = (1/2)(\partial u/\partial y + \partial v/\partial x)$ , etc.] yields the strains:

$$\begin{aligned} \epsilon_{xx} &= 0, \quad \epsilon_{yy} = 0, \quad \epsilon_{zz} = 0, \quad \epsilon_{xy} = 0 \\ \epsilon_{yz} &= \frac{1}{2}\theta \left( \frac{\partial \psi}{\partial y} + x \right), \quad \epsilon_{zx} = \frac{1}{2}\theta \left( \frac{\partial \psi}{\partial x} - y \right) \end{aligned} \quad (4)$$

### STRESS ANALYSIS

Since the only non-zero strains are  $\epsilon_{xx}$  and  $\epsilon_{yz}$ , linear elasticity conditions yield that the only non-zero stress components are:

$$\sigma_{xx} = 2G\epsilon_{xx} \quad \text{and} \quad \sigma_{yz} = 2G\epsilon_{yz} \quad (5)$$

Using the fundamental equation of infinitesimal equilibrium yields:

$$\frac{\partial \sigma_{xx}}{\partial x} + \frac{\partial \sigma_{yz}}{\partial y} = 0 \quad (6)$$

Equation (5) implies the existence of a potential function, called the *Prandtl stress function*,  $\phi(x,y)$ , such that:

$$\sigma_{xx} = \frac{\partial \phi}{\partial y}, \quad \sigma_{yz} = -\frac{\partial \phi}{\partial x} \quad (7)$$

Analysis of the boundary equilibrium condition in the cross-section indicates that the Prandtl stress function,  $\phi(x,y)$  must be constant along the cross-section's contour,  $S$ , and hence  $\phi(x,y) = 0$  on  $S$ . Applying the general static equilibrium condition of the cross-section yields:

$$T = 2 \iint \phi dx dy \quad (8)$$

The strain expressions given in Equation (4) can be processed to eliminate the function  $\psi$ , thus yielding the strain compatibility condition:

$$\frac{\partial \epsilon_{yz}}{\partial x} - \frac{\partial \epsilon_{zx}}{\partial y} = \theta \quad (9)$$

Using Equation (5) of linear elasticity and Equation (7) defining the stresses in terms of the Prandtl stress function,  $\phi(x,y)$ , yields the differential equation for the stress function:

$$\frac{\partial^2 \phi}{\partial x^2} + \frac{\partial^2 \phi}{\partial y^2} = -2G\theta \quad (10)$$

### THIN-WALL OPEN-TUBE SOLUTION

For thin-wall sections, the Prandtl stress function has the general solution (Goodier, 1962; Boresi et al., 1993):

$$\phi(n) = G\theta \left( \frac{r^2}{4} - n^2 \right) \quad (11)$$

where  $n$  is the normal to the open section contour,  $\Gamma$ . Using Equation (7) with coordinates  $x$  and  $y$  replaced by  $n$  and  $s$  (Figure 3), yields:

$$\tau_s(n) = \sigma_{yz} = \frac{\partial \phi}{\partial n} = -2G\theta n \quad (12)$$

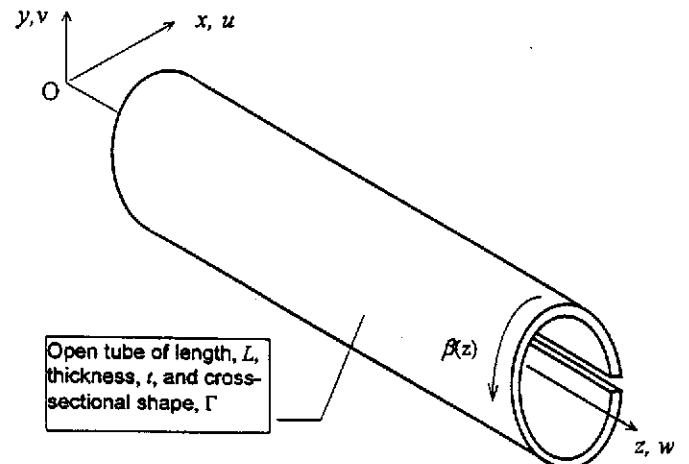


Figure 2. Schematic representation of an open tube under torsion.

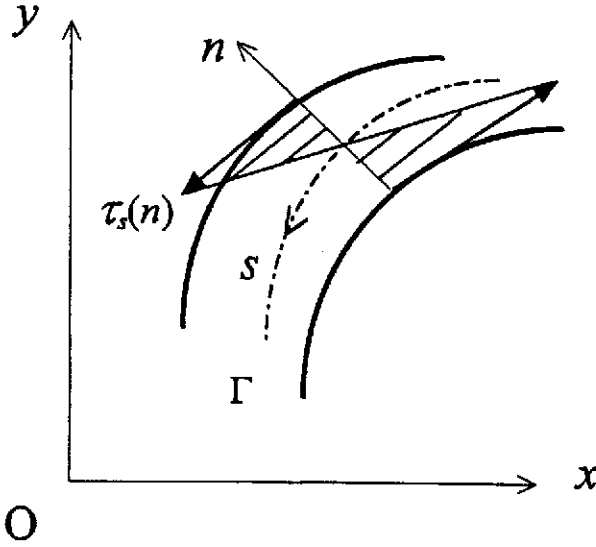


Figure 3. Distribution of shear stresses inside an open tube cross-section.

Equation (12) shows that the shear stress,  $\tau(n)$ , is constant along the section contour,  $\Gamma$ , and varies linearly across the thickness,  $t$ . On the mid-thickness contour,  $\Gamma$ , the shear stress is zero ( $\tau(0) = 0$ ). Equations (8) and (11) give the torque expression:

$$T = G \frac{I t^3}{3} \theta \quad (13)$$

where  $I$  is the length of section contour,  $\Gamma$ . Equations (13) and (12) allow us to estimate the maximum shear stress,  $\tau_{\max}$ , which takes place at the outer fibers ( $n = \pm t/2$ ), i.e.,

$$\tau_{\max} = \frac{3T}{I t^2} \quad (14)$$

Equation (13) can be recast in the familiar expression:

$$T = GJ\theta \quad (15)$$

where  $GJ$  is the effective torsional stiffness, i.e.,

$$J = \frac{I t^3}{3} \quad (16)$$

#### TWIST-WARPING SOLUTION FOR A THIN-WALL OPEN TUBE

Assume an infinitesimal arc increment,  $ds$ , along the mid-thickness contour,  $\Gamma$ , and the corresponding coordinate increments,  $dx$  and  $dy$ , such that  $d\vec{s} = \vec{i} dx + \vec{j} dy$ . Hence, for an incremental arc,  $ds$ , the incremental warping per unit twist is:

$$d\psi = \frac{\partial \psi}{\partial x} dx + \frac{\partial \psi}{\partial y} dy \quad (17)$$

Equations (4) yields

$$\frac{\partial \psi}{\partial y} = \frac{2\varepsilon_{yz}}{\theta} - x, \quad \frac{\partial \psi}{\partial x} = \frac{2\varepsilon_{zx}}{\theta} + y \quad (18)$$

Using Equation (5) in Equation (18), and substituting the result into Equation (17) yields:

$$d\psi = \left( \frac{\sigma_{zx}}{G\theta} + y \right) dx + \left( \frac{\sigma_{yz}}{G\theta} - x \right) dy \quad (19)$$

Equation (19) is conveniently rearranged as:

$$d\psi = \frac{1}{G\theta} (\sigma_{zx} dx + \sigma_{yz} dy) + (y dx - x dy) \quad (20)$$

It can be easily shown (Goodier, 1962) that the first term in Equation (20) can be identified with the shear stress,  $\tau_s(n)$ , i.e.,

$$\tau_s(n) = \sigma_{zx} dx + \sigma_{yz} dy \quad (21)$$

and, on the mid-thickness contour,  $\Gamma$ ,  $\tau_s(n) = 0$ . The second term in Equation (20) can be expressed using polar coordinates  $x = r \cos \alpha$ ,  $y = r \sin \alpha$ , as:

$$-r \cdot d\vec{s} = (y dx - x dy) \quad (22)$$

where  $\vec{r} \cdot d\vec{s} = r^2 d\alpha$ . Hence, on the mid-thickness contour,  $\Gamma$ , the warping function infinitesimal increment is:

$$d\psi = -\vec{r} d\vec{s} \quad (23)$$

Integration of Equation (23) gives:

$$\Delta\psi = \psi(0) - \psi(l) = \int_0^l \vec{r} d\vec{s} \quad (24)$$

Equation (24) represents the relative warping per unit twist between the two edges of the open section. For an open section where the two edges are closed together, the curve  $\Gamma$  is almost closed. The swept area enclosed by  $\Gamma$  is denoted by  $A$ . Hence, the integral in Equation (24) can be approximated by  $2A$ , and the relative warping per unit twist of the cross-section is given by the simple approximation:

$$\Delta\psi \approx 2A \quad (25)$$

According to Equations (2) and (25), the relative displacement of the two edges of the open tube is,

$$\Delta w \approx 2A\theta \quad (26)$$

Substitution of Equation (26) into the definition  $\beta(z) = \theta z$  yields the twist-warping coupling equation:

$$\beta(z) = \frac{z}{2A} \Delta w \quad (27)$$

#### LINEAR-TO-ANGULAR CONVERTER-AMPLIFIER CONCEPT

Using Equation (27), we obtain the total angular rotation,  $\delta = \beta(L)$ , between the two ends of an open tube:

$$\delta = \frac{L}{2A} \Delta w \quad (28)$$

where  $L$  is the length of the open tube,  $A$  is the area enclosed by the almost-closed cross-section of the tube, and  $\Delta w$  is the relative displacement between the two edges of the tube. Equation (28), describing the *linear-to-angular converter and amplifier effect* of a thin-wall open tube represents the *quintessence* of our claim. Equation (28) can be successfully used to construct an effective solid-state axial-to-rotary converter and displacement amplifier. The conversion-amplification factor,

$$\frac{\partial \delta}{\partial (\Delta w)} = \frac{L}{2A} \quad (28a)$$

is shown to increase with the increase in the length,  $L$ , and with the decrease in the enclosed area,  $A$ .

#### LARGE-AMPLITUDE ROTARY INDUCED-STRAIN (LARIS) ACTUATOR

By applying an induced-strain axial displacement at the root of the open tube, one obtains a large-amplitude rotary induced-strain (LARIS) actuator. According to Equation (28a), the amplification of the LARIS actuator can be increased by either a longer length, or a smaller enclosed area through a reduced diameter.

The stiffness of the LARIS actuator,  $GJ$ , is controlled by Equation (16), which involves the circumferential length,  $l = \pi D$ , and the cube of the wall thickness,  $t$ . The fact that the stiffness,  $GJ$ , and the conversion-amplification ratio,  $\partial \delta / \partial (\Delta w)$ , are controlled by different parameters offers extensive design opportunities for the LARIS actuator. It can be envisaged that, with proper use of the material, and with a cellular or sandwich-wall construction, a very large design space can be encompassed.

## EXPERIMENTAL RESULTS

### Description of the Test Specimen

To test the validity of the proposed solid-state axial-to-rotary converter-amplifier, a proof-of-concept demonstrator was built and tested in the CIMSS laboratory. The proof-of-concept demonstrator consisted of a 28 mm diameter, 1.2 m long steel open tube with 0.8 mm wall thickness, actuated by

a Polytec PI P-245.70 PZT translator with a nominal stroke of 120  $\mu\text{m}$  at  $-1000$  V. The open tube performs the function of the solid-state axial-to-rotary converter-displacement amplifier, while the P-245.70 PZT translator produces the induced-strain input displacement. The assembly of the open-tube solid-state converter-amplifier and the PZT translator forms the proof-of-concept demonstrator of a large-amplitude induced-strain rotary (LARIS) actuator. The connection between the PZT translator and the open-tube converter-amplifier is only unilateral, i.e., the head of the PZT translator rests directly against a recess in the end of the open-tube converter-amplifier. To ensure positive contact throughout the operation range, the PZT translator is pre-loaded in compression against the warping-torsion stiffness of the open-tube converter-amplifier. The pre-loading is done through the mounting screw. This pre-load also ensures positive compression stress on the PZT translator, and thus prevents premature failure and increases the fatigue life.

### Description of the Excitation and Measuring Equipment

The testing of the LARIS actuator was performed using the experimental set-up presented in Figure 1. The excitation of the P-245.70 PZT translator was performed using a TREK 50/750 high-voltage amplifier driven by an HP 3314A low-voltage function generator. The function generator was used to create a low-voltage input signal in the range  $-10$  V to  $+1$  V. The low-voltage signal was sent to the high-voltage amplifier and also monitored on channel A of a JDR 2000 oscilloscope. The high-voltage amplifier raised the voltage level of the low-voltage signal 100 times. The amplified signal, covering the range  $-1000$  V to  $+100$  V, was sent to the P-245.70 PZT translator and, for monitoring, to channel B of JDR 2000 oscilloscope through a 10:1 reduction probe. The low-voltage and high-voltage signals were displayed simultaneously on the oscilloscope screen. Comparison of the simultaneously displayed signals ensured proper monitoring of the waveform, and identification of possible amplification distortions. Waveform distortion was noticed only when the positive voltage exceeded  $+100$  V, which was outside the  $-1000$  V to  $+100$  V operating range of the experiment.

The measuring instrumentation consisted of a high-precision Solatron DF 1.0 LVDT displacement transducer and a set of 4 arm-and-scale rotation measuring devices. The displacement transducer was used to record the relative displacement,  $\Delta w$ , expected to vary in the range  $-12$   $\mu\text{m}$  to  $120$   $\mu\text{m}$ . The arm-and-scale rotation measuring devices consisted of 4 light-weight 150 mm rotor arms affixed to the open-tube at 0.3 m (1-ft) intervals, and of 4 vertical rulers for reading the vertical position of the arm tips. A detail of the angle-measurement principle is given also in Figure 4.

### Experimental Procedure

#### EVALUATION OF THE PZT TRANSLATOR

A simple experiment was first conducted to evaluate the

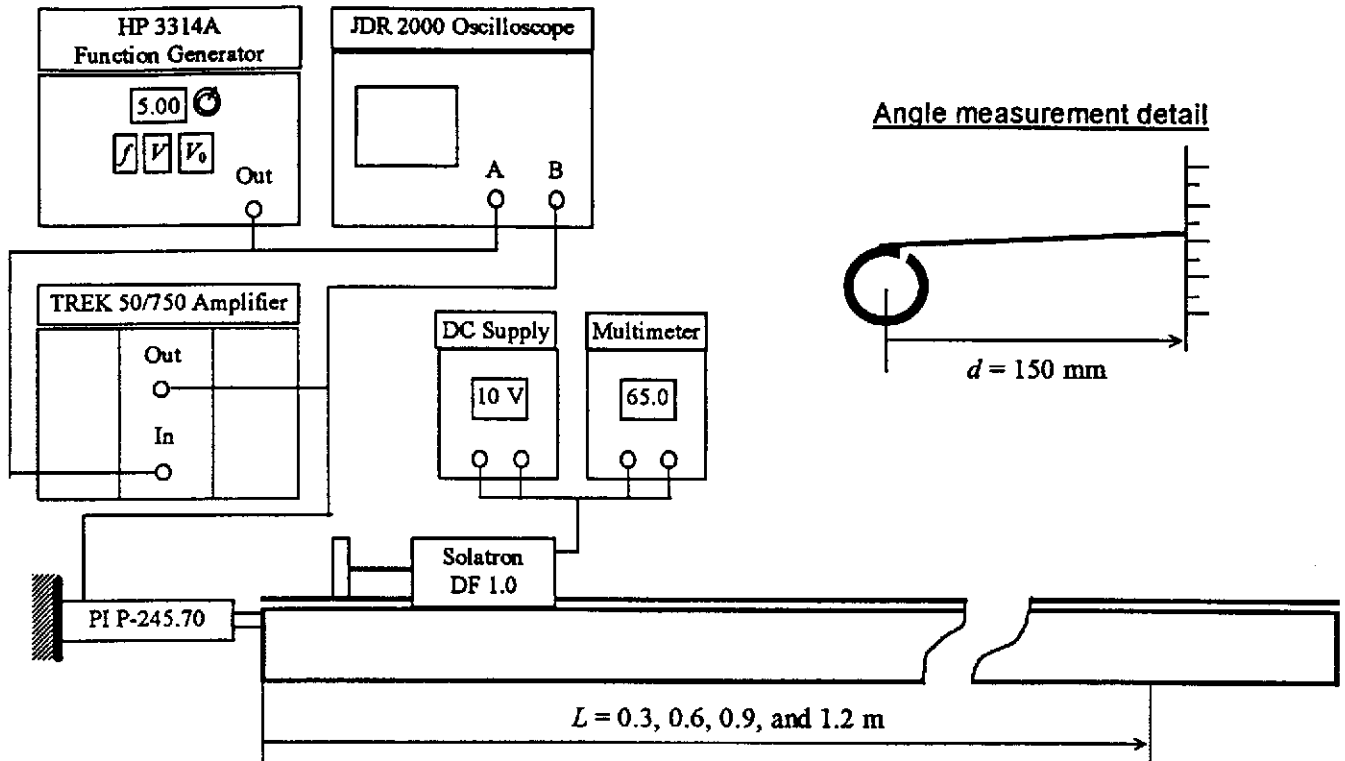


Figure 4a. Experimental set-up for the LARIS actuator proof-of-concept demonstrator: (a) schematic diagram.

voltage-displacement behavior of the P-245.70 PZT translator. For this purpose, the PZT translator was placed separately on the bench. The DF 1.0 displacement transducer was coupled directly to the end of the PZT translator. Starting from zero, the excitation voltage to the P-245.70 PZT translator was raised in steps of  $-200$  V up to the maximum value of  $-1000$  V, and then gradually decreased back to zero. Next, the voltage was taken to  $+100$  V, and then brought back to zero. The complete cycle was repeated one more time. At each step, complete readings of the excitation voltage,  $V_{in}$ , and of the displacement transducer output,  $V_{ISA}$ , were taken and recorded.

#### EVALUATION OF THE LARIS ACTUATOR

The P-245.70 PZT translator was placed at the root end of the LARIS actuator, as shown in Figure 4. Starting from zero,

the excitation voltage to the P-245.70 PZT translator was raised in steps of  $-200$  V up to the maximum value of  $-1000$  V, and then gradually brought back to zero, in steps of  $200$  V. Next, the voltage was taken to  $+100$  V, and then returned to zero. The complete cycle was repeated one more time. At each step, complete readings of the excitation voltage,  $V_{in}$ , displacement transducer output,  $V_{ISA}$ , and the vertical positions of the 4 rotor-arm tips,  $z_1, \dots, z_4$ , were taken and recorded.

#### DISCUSSION OF RESULTS

##### Data Processing and Interpretation

Data processing was performed using the MS-Excel software. The initial data, recorded at zero excitation voltage,

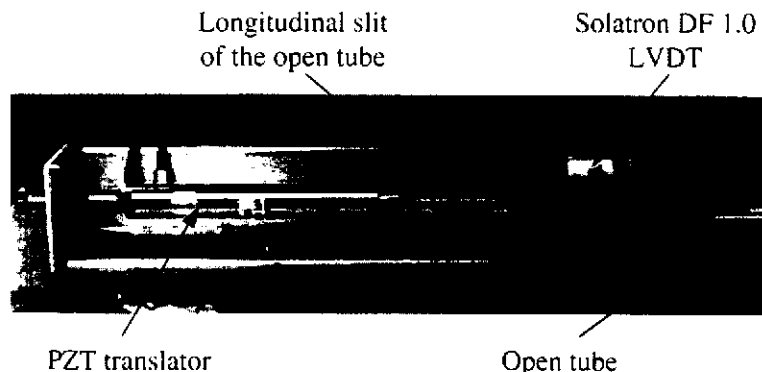


Figure 4b. Close-up photograph of the experimental set-up showing details of the mechanical connections.

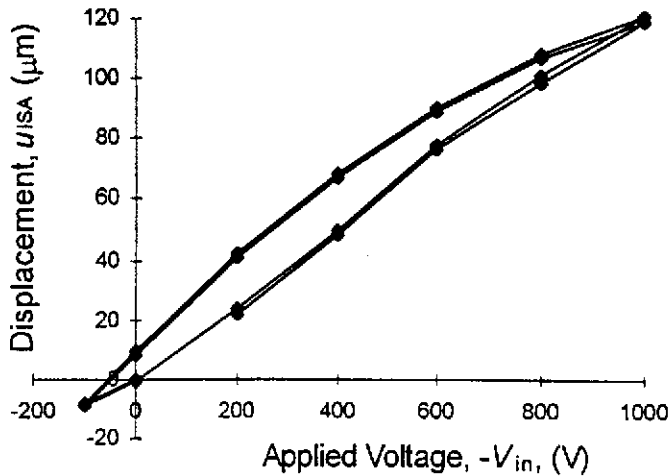


Figure 5. The induced-strain linear displacement vs. applied voltage curve of the PI P-245.70 PZT translator.

were taken as datum and the incremental values of each data series were calculated. The LVDT calibration factor was used to compute the actual input displacement,  $u_{ISA}$ . The  $\delta = \sin^{-1}(\Delta z/d)$  relationship, with  $d = 150$  mm, was used to calculate the rotation angles,  $\delta_1, \dots, \delta_4$ . The processed data was plotted as graphs of the input displacement vs. excitation voltage, and of the rotation angles vs. input displacement.

Figure 5 presents the induced-strain linear displacement vs.

applied voltage for the PI P-245.70 PZT translator. Examination of the curve in Figure 5 reveals the following aspects:

- A maximum induced-strain linear displacement of  $120 \mu\text{m}$  is consistently obtained.
- The voltage-displacement curve is highly repetitive, thus laying the premise for good repeatability of the complete LARIS device.
- The charge-discharge cycle of the PI P-245.70 PZT translator displays significant hysteresis in the mechanical response. This behavior is inherent in the PZT material; it may be improved by using other electro-active materials that display better linearity (e.g., the EC-98 PMN from EDO Corporation).

Figure 6 presents the rotation angle vs. input displacement curves for sections placed at various stations along the length of the open-tube converter-amplifier. Examination of the curves in Figure 6 reveal the following aspects:

- The curves have good linearity, thus ensuring that the behavior of the solid-state converter-amplifier is within the linear range.
- The curves are repetitive, thus laying the premise for good repeatability of the complete LARIS device.
- The rotation angle increases with the tube length. At  $L_1 = 0.3$  m, the maximum peak-to-peak rotation is around  $\delta_1 =$

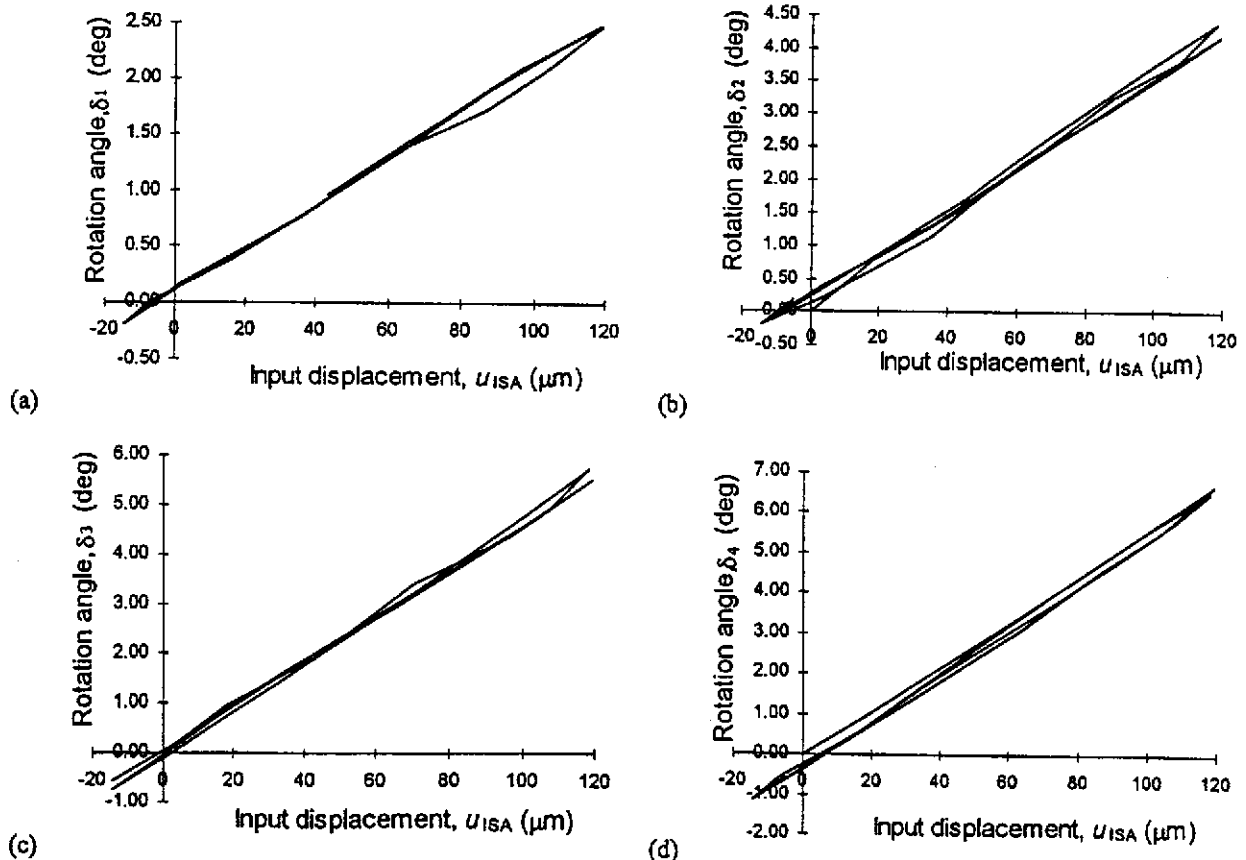


Figure 6. Rotation angle vs. input displacement at various stations along the open-tube converter-amplifier: (a)  $\delta_1$  at  $L_1 = 0.3$  m; (b)  $\delta_2$  at  $L_2 = 0.6$  m; (c)  $\delta_3$  at  $L_3 = 0.9$  m; (d)  $\delta_4$  at  $L_4 = 1.2$  m.

2.5°; at  $L_2 = 0.6$  m it is  $\delta_2 = 4.5^\circ$ ; at  $L_3 = 0.9$  m it is  $\delta_3 = 6.5^\circ$ ; and at  $L_4 = 1.2$  m it is  $\delta_4 = 8^\circ$ . This behavior is consistent with the behavior predicted by Equation (28).

To obtain complete understanding of how well Equation (28) predicts the behavior of the LARIS actuator, a further data-processing step was applied. The curves in Figure 6 were fitted with straight lines using a linear regression procedure. The coefficients of linear regressions,  $m_1, \dots, m_4$ , represent the output rotation per unit input displacement (deg/mm). These coefficients were plotted against the actuator length,  $L$ , in Figure 7. Examination of Figure 7 shows that the four data points fall almost exactly on the straight line of the equation  $(8.8 + 41 \cdot L)$  deg/mm, i.e.,

$$\left( \frac{\partial \delta}{\partial (\Delta w)} \right)_{\text{exp}} = (8.8 + 41.0 \cdot L) \text{ deg/mm} \quad (29)$$

For comparison, we differentiate Equation (28) with respect to  $\Delta w$ , and write:

$$\left( \frac{\partial \delta}{\partial (\Delta w)} \right)_{\text{theory}} = \frac{1}{2A} \cdot L \quad (30)$$

Further differentiating Equations (29) and (30) with respect to  $L$  yields:

$$\left( \frac{\partial \delta}{\partial (\Delta w) \partial L} \right)_{\text{exp}} = 41.0 \text{ deg/mm/m} \quad (31)$$

and

$$\left( \frac{\partial^2 \delta}{\partial (\Delta w) \partial L} \right)_{\text{theory}} = \frac{1}{2A} \quad (32)$$

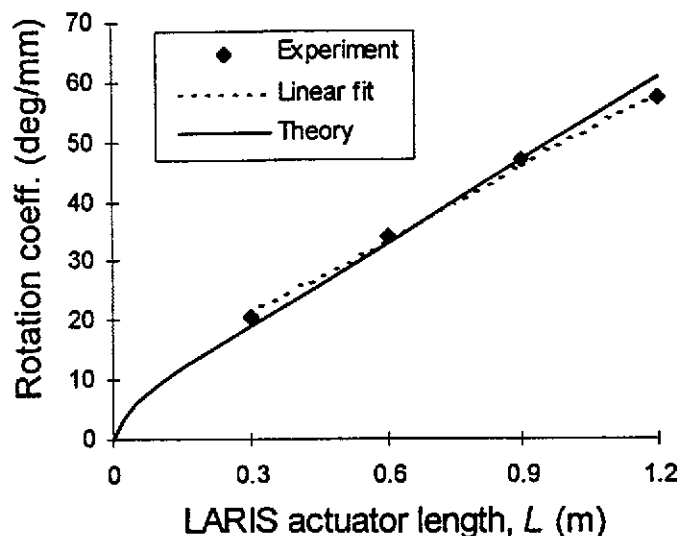


Figure 7. The converter-amplifier rotation coefficient vs. LARIS actuator length.

Calculation of the quantity  $1/2A$  for the open tube with  $D = 28$  mm yields the value  $812 \text{ rad/m}^2 = 46.6^\circ/\text{mm/m}$ . It can be seen that this value agrees with Equation (31) within 12%.

### Improvement of the Theoretical Model

In the previous section, we have proven that the linear behavior predicted by Equation (28) has been satisfactorily confirmed by the experimental data taken at  $L = 0.3, 0.6, 0.9$  and  $1.2$  m. However, a closer examination of Figure 7 reveals that the experimental data would not predict that  $\theta \rightarrow 0$  as  $L \rightarrow 0$ . This apparent violation of the initial theory was given further examination. Analysis of the boundary conditions reveals that the left-hand side of the open tube is subjected to restraint warping and other effects associated with the detailed mechanical design of the root end of the LARIS actuator. Thus, additional constraints are posed on the root section of the LARIS actuator which compel its behavior to depart from the simple free-torsion linear theory. The analytical solution for the torsion of an open tube with warping constraints at the built-in end is given by Goodier (1962) in the general form:

$$\delta = \frac{T}{GJ} [x - (1 - ae^{-(x/a)})] \quad (33)$$

where  $a = ET/GJ$  is the length scale of the exponential asymptotic behavior, and  $\Gamma$  is the second torsional constant of the cross-section, i.e., the *warping integral*. Examination of the detailed mechanical design of the LARIS actuator root section reveals that fully built-in conditions do not apply, since some relative movement is permitted in order to introduce the PZT actuator input,  $\Delta w$ . Hence, Equation (33) cannot be applied directly. However, an empirical correction to the linear theory can be searched following the general features of Equation (33). By doing this, we developed the expression:

$$\delta = (1 - e^{-L/L_0}) \left( \delta'_0 + \frac{L}{2A} \right) \Delta w \quad (34)$$

where  $\delta'_0$  is the zero off-set, and  $L_0$  is a length scale. Fitting Equation (34) to the experimental data, yielded  $\delta'_0 = 5^\circ/\text{mm}$  and  $L_0 = D$ . These values, when substituted in Equation (34) gave the results shown by the "theory" line of Figure 7. Thus, good agreement between the experimental results and the theory, in its modified form of Equation (34), was achieved.

### CONCLUSIONS

A new concept has been proposed for obtaining large-amplitude rotary displacements from the small linear displacements generated by induced-strain active materials. The concept utilizes the theory of twist-warping coupling in thin-wall

open tubes. Complete development of this theory, together with the appropriate bibliographical references, is given. The estimation of the axial-to-rotary conversion-amplification coefficient from the geometrical length,  $L$ , and enclosed area,  $A$ , of the open tube is given through the remarkably simple Equation (28).

The large-amplitude rotary induced-strain (LARIS) proof-of-concept demonstrator, was built to verify and validate the theoretical developments. The LARIS actuator consisted of a 28 mm diameter, 1.2 m length open tube and a 120  $\mu\text{m}$ , -1000 V PZT translator. The open tube served as a solid-state axial-to-rotary converter-amplifier, while the PZT translator provided the induced-strain actuation. The proof-of-concept demonstrator was subjected to extensive testing in the CIMSS laboratory. The experimental set-up and the excitation and measuring equipment was fully described.

Processing of the recorded data revealed the expected behavior of both the induced-strain PZT translator and of the solid-state axial-to-rotary converter-amplifier. A maximum rotary displacement of  $8^\circ$  was measured. The linear relationship between the rotation coefficient, the tube length,  $L$ , and the inverse of the enclosed area,  $A$ , was verified. Following the interpretation of the experimental results, an improved theoretical model was developed to account for the zero off-set observed in the  $L$ -variation of the rotation coefficient. This zero off-set is attributed to the restrained warping and other non-linear constraints present in the root section of the LARIS actuator. The improved theoretical model, Equation (34), predicts very well the observed behavior over the full length of the device.

Through theoretical developments and experimental tests, this paper has shown that the proposed LARIS actuator, based on a novel solid-state axial-to-rotary converter-amplifier utilizing the warping-torsion coupling of an open tube, is a viable design option, of great constructive simplicity and very low parts count. This concept can be successfully used in a series of aerospace and mechanical engineering applications, as for example in the actuation of adaptive control surfaces for aircraft wings and helicopter blades. The  $8^\circ$  rotary displacement capabilities measured on the proof-of-concept demonstrator can be easily scaled to other values to meet the operation requirements of specific applications. Future work on the LARIS concept should investigate the stiffness-displacement-energy relationship in order to develop a complete design guide for this novel induced-strain rotary actuator.

It should be also noted that the application range of the solid-state axial-to-rotary converter and displacement amplifier concept are not limited to induced-strain actuation. In fact, larger rotary displacements, but at lower frequencies, can be obtained using conventional electro-mechanical actuators (e.g., steppers-motors and ball-screws assemblies). Preliminary experiments have shown that angles of  $40$ – $50^\circ$  can be readily obtained.

It should be also pointed out that the open-tube actuation solution proposed in this paper is not a good-for-all *panacea*. For the same geometry and wall thickness, open tubes are

more flexible in torsion than closed tubes, and they can bear less torsional loads. These effects, though potential drawbacks, can be compensated through the use of different wall thicknesses and/or high-performance composite materials with orthotropic properties. Tailoring of composite material properties coupled with design optimization to meet specific application requirements can be performed, and such a task, though requiring extended research effort, would be a worthwhile extension of the present analysis.

## ACKNOWLEDGEMENTS

The research reported in this paper was initiated while the authors were with the Center for Intelligent Material Systems and Structures at Virginia Polytechnic Institute and State University. The authors gratefully acknowledge the support of the U.S. Army Research Office–University Research Initiative Program, Grant No. DAAL03-92-0181, Dr. Gary Anderson, Program Manager.

## REFERENCES

- Anon. 1995. *PI Products for Micropositioning*. Polytec PI, Inc.: Auburn, MA 01501.
- Barrett, R., R. S. Gross and F. Brozoski. 1995. "Missile Flight Control Using Active Flexspar Actuators", *Smart Structures and Materials 1995—Smart Structures and Integrated Systems*, SPIE, Vol. 2443, pp. 52–61.
- Bernhard, A. P. F. and I. Chopra. 1996. "Hover Testing of a Smart Flap Activated by a Bending-Torsion Coupled Beam", *Proceedings of the 37th AIAA/ASME/ASCE/AHS/ASC Structures, Structural Dynamics and Materials Conference and Adaptive Structures Forum*, Salt Lake City, UT, April 15–19, #AIAA-946-11272-CP.
- Boresi, A. P., R. J. Schmidt and O. M. Sidebottom. 1993. *Advanced Mechanics of Materials*, 5th Edition. John Wiley & Sons, pp. 237–292.
- Bothwell, C. M., R. Chandra and I. Chopra. 1994. "Torsional Actuation with Extension-Torsion Composite Coupling and Magnetostrictive Actuators," *Proceedings of the 35th AIAA/ASME/ASCE/AHS/ASC Structures, Structural Dynamics and Materials Conference and Adaptive Structures Forum*, Hilton Head, SC, April 18–21, 1994, #AIAA-94-1760-CP.
- Chen, P. C. and I. Chopra. 1993a. "A Feasibility Study to Build a Smart Rotor: Induced-Strain Actuation of Airfoil Twisting Using Piezoceramics", *Proceedings of the 1993 North American Conference on Smart Structures and Materials*, Paper 1917-20, Hyatt Regency Hotel, Albuquerque, New Mexico, 31 January–4 February.
- Fenn, R. C., J. R. Downer, D. A. Bushko, D. A., V. Gondhalekar and N. D. Ham. 1993. "Terfenol-D Driven Flaps for Helicopter Vibration Reduction", Paper #0-8194-1150-7/93, *Smart Structures and Intelligent Systems (1993)*, SPIE, Vol. 1917, pp. 407–418.
- Giurgiutiu, V., Z. Chaudhry, C. A. Rogers. 1994. "Engineering Feasibility of Induced-Strain Actuators for Rotor Blade Active Vibration Control", *Smart Structures and Materials '94*, Orlando, FL, 13–18 February, Paper # 2190-11, SPIE, Vol. 2190, pp. 107–122.
- Giurgiutiu, V., Z. Chaudhry and C. A. Rogers. 1996. "Energy-Based Comparison of Solid-State Induced-Strain Actuators", *Journal of Intelligent Material Systems and Structures*, 7(1):4–14.
- Goodier, J. N. 1962. "Torsion", in *Handbook of Engineering Mechanics*, W. Flugge, ed., McGraw Hill, pp. 36–118.
- Samak, D. K. and I. Chopra. 1993. "A Feasibility Study to Build a Smart Rotor: Trailing Edge Flap Actuation", *Proceedings of the 1993 North*

- American Conference on Smart Structures and Materials*, Paper 1917-20, Hyatt Regency Hotel, Albuquerque, New Mexico, 31 January–4 February.
- Spangler, R. L., Jr., and S. R. Hall. 1990. "Piezoelectric Actuators for Helicopter Rotor Control", *Proceedings of the AIAA/ASME/ASCE/AHS/ASC 31st Structures, Structural Dynamics, and Materials Conference*, Long Beach, CA, April 1990, Paper AIAA-90-1076-CP, pp. 1589–1599.
- Spencer, B. T. and I. Chopra. 1996. "Design of a Helicopter Trailing Edge Flap with Piezoelectric Stack Actuators", *Smart Structures and Materials 1996—Smart Structures and Integrated Structures*, SPIE, Vol. 2717, pp. 120–131.
- Straub, K. and R. King. 1996. "Applications of Smart Materials to Control of a Helicopter Rotor", *Smart Structures and Materials 1996—Industrial and Commercial Applications of Smart Structures Technology*, SPIE, Vol. 2721, pp. 66–77.